Photoinduced Carrier Generation and Decay Dynamics in Intercalated and Non-intercalated Polymer:Fullerene Bulk Heterojunctions

William L. Rance,[†] Andrew J. Ferguson,[‡] Thomas McCarthy-Ward,[§] Martin Heeney,[§] David S. Ginley,[‡] Dana C. Olson,[‡] Garry Rumbles,[‡] and Nikos Kopidakis[‡,*]

[†]Department of Physics, Colorado School of Mines, 1523 Illinois Street, Golden, Colorado 80401, United States, [‡]National Renewable Energy Laboratory, 1617 Cole Boulevard, Golden, Colorado 80401, United States, and [§]Department of Chemistry, Imperial College London, South Kensington, SW7 2AZ, United Kingdom

ABSTRACT The dependence of photoinduced carrier generation and decay on donor–acceptor nanomorphology is reported as a function of composition for blends of the polymer poly(2,5-bis(3-tetradecylthiophen-2-yl)thieno[3,2-*b*]thiophene) (pBTTT-C_{14}) with two electron-accepting fullerenes: phenyl-C_{71}-butyric acid methyl ester ($PC_{71}BM$) or the bisadduct of phenyl-C_{61}-butyric acid methyl ester (bis-$PC_{61}BM$). The formation of partially or fully intercalated bimolecular crystals at weight ratios up to 1:1 for pBTTT-C_{14}:$PC_{71}BM$ blends leads to efficient exciton quenching due to a combination of static and dynamic mechanisms. At higher fullerene loadings, pure $PC_{71}BM$ domains are formed that result in an enhanced free carrier lifetime, as a consequence of spatial separation of the electron and hole into different phases, and the dominant contribution to the photoconductance comes from the high-frequency electron mobility in the fullerene clusters. In the pBTTT-C_{14}:bis-$PC_{61}BM$ system, phase separation results in a non-intercalated structure, independent of composition, which is characterized by exciton quenching that is dominated by a dynamic process, an enhanced carrier lifetime and a hole-dominated photoconductance signal. The results indicate that intercalation of fullerene into crystalline polymer domains is not detrimental to the density of long-lived carriers, suggesting that efficient organic photovoltaic devices could be fabricated that incorporate intercalated structures, provided that an additional pure fullerene phase is present for charge extraction.

KEYWORDS: conjugated polymer · fullerene · intercalation · photoconductance · electron transfer · blend

Research in solution-processable organic photovoltaics (OPV) has produced remarkable advances in efficiency.[1−4] These devices are amenable to "roll-to-roll" deposition by simple spraying[5−7] or printing[8,9] methods that promise to drive down production costs and close the price gap between solar electricity and that produced by fossil fuels.[10] The active, light-absorbing layer of OPV devices is typically a composite of a conjugated polymer and a fullerene derivative, deposited from a blend solution. A photon absorbed in the polymer generates an exciton that must diffuse to an interface between the polymer (donor) and the fullerene (acceptor) to dissociate into free, uncorrelated carriers: a hole in the polymer and an electron in the fullerene,[11,12] although ultrafast (subpicosecond) carrier generation has also been observed in these systems.[13,14] Due to the short exciton diffusion lengths of 5−10 nm in typical conjugated polymers,[2,4] it is necessary for the donor−acceptor interface to extend throughout the active layer on length scales comparable to the exciton diffusion length, hence the term "bulk heterojunction" that is used to denote this approach. The morphology of the nanostructured active layer also plays an important role in the extraction of photogenerated electrons and holes from the device: the polymer and the fullerene must each form a percolation network for their respective charge carriers to be extracted from the device before recombining. For these reasons, there is general consensus that the morphology of the active layer at the nanometer scale is one of the major determinants of their photovoltaic performance, and considerable effort has been devoted to understanding the often complex morphology−performance relationships observed in these donor−acceptor systems.[2,15−17]

The requirement of solution processability for inexpensive devices makes direct control of their morphology difficult, as one cannot precisely predict the nanostructure that a polymer−fullerene composite will adopt after the solvent dries. In fact, there are only a limited number of examples demonstrating *a priori* knowledge of how to control the microstructure of blended systems containing conjugated polymers,[18] and generally the effect of processing

* Address correspondence to nikos.kopidakis@nrel.gov.

Received for review April 4, 2011 and accepted June 8, 2011.

Published online June 08, 2011
10.1021/nn201251v

conditions on the final morphology is determined after film formation is complete. To add further complexity to this problem, the conjugated polymers that have been employed as active photovoltaic components can be separated into two broad structural categories: amorphous and semicrystalline.[19]

The earliest OPV devices utilized blends containing soluble derivatives of poly(phenylene vinylene) and fullerene derivatives as the donor and acceptor, respectively.[8,20−22] The polymers in these devices adopt an amorphous structure with only short-range interchain interactions,[22] producing mixed polymer−fullerene domains that surround pure fullerene regions.[23,24] More recently, several semicrystalline polymers have emerged as efficient light-absorbing and electron-donating materials for OPV,[19,25−27] which has facilitated the detailed investigation of the structure of donor−acceptor blends with techniques such as X-ray diffraction (XRD) and the derivation of relationships between the active layer morphology and optical properties,[28−30] and ultimately the solar photoconversion performance.[2,17,28] A prominent polymer in this class is poly(3-hexylthiophene) (P3HT); XRD studies have shown that ordered nanodomains of pure polymer are present in partially phase-separated P3HT:$PC_{61}BM$ films[28] and that $PC_{61}BM$ is excluded from these domains.[28,31] The resulting morphology seems ideal for charge carrier percolation as is verified from internal quantum efficiencies in devices that reach ~90%.[32] However, amorphous domains of P3HT also exist in films[15,16,28,30,33,34] and it is a reasonable assumption that because of their disordered structure the spatial constraints that cause exclusion of $PC_{61}BM$ from crystalline polymer domains[35] are now partially or fully relaxed, resulting in a finely mixed blend in these regions.[15,16,28,30,33,34] It has been proposed that this mixed phase plays an important role in exciton dissociation in this system,[18,36] although little conclusive experimental evidence is currently available.

Despite this progress, there is still limited information available regarding the dynamics of photoinduced electron and hole generation and recombination as a function of active layer morphology, particularly with respect to the effects of mixed or separated polymer and fullerene phases. For example, in systems that contain finely mixed polymer−fullerene domains that coexist with domains of the pure components, it remains unclear what the relative importance of each type of domain is in determining the lifetimes of photoinduced carriers.

In a recent work, Mayer *et al.* used XRD to determine the morphology of composites of the polymer poly(2,5-bis(3-tetradecylthiophen-2-yl)thieno[3,2-*b*]-thiophene) (pBTTT-C_{14}) with a low loading of $PC_{71}BM$ and were able to demonstrate that the structure of the composite at the molecular level consisted of fullerenes intercalated within the ordered polymer chains, forming a *bimolecular crystal*.[35] At a weight ratio of 1:1, the polymer is fully intercalated; that is, all available sites for fullerene intercalation have been filled. At higher fullerene loadings, it was shown that the $PC_{71}BM$ forms pure fullerene domains outside the bimolecular crystal; these domains are essential for electron percolation in OPV devices—the best device efficiency of 2.51% is reached at a loading of 1:4 pBTTT:$PC_{71}BM$ for the hexadecyl-substituted pBTTT polymer, pBTTT-C_{16}.[37] Further control of the morphology of pBTTT:fullerene blends can be achieved by using a bisadduct of $PC_{71}BM$ (bis-$PC_{71}BM$). In this case, there is no intercalation because the additional solubilizing group means that the fullerene is too large to fit between polymer side chains, and separation of polymer and fullerene is observed.[37] We will show that the bisadduct of $PC_{61}BM$ (bis-$PC_{61}BM$) can be used as an analogue for bis-$PC_{71}BM$ electron acceptor because identical separation of the components occurs. In summary, by using *a single polymer* in conjunction with the appropriate fullerene derivative and blending ratio, one can produce *any ordered nanomorphology* that is of interest to understanding and controlling the performance of OPV: a partially (10:1 bw pBTTT:$PC_{71}BM$) or fully intercalated phase (1:1 pBTTT:$PC_{71}BM$), coexisting intercalated phase and pure fullerene domains (1:4 pBTTT:$PC_{71}BM$), and separate pure polymer and pure fullerene domains (pBTTT:bis-$PC_{71}BM$ at any blending ratio).[35,37] This tunability of pBTTT:fullerene blends makes them an excellent model system to study the location and transport properties of free carriers and to investigate the correlation between the nanoscale morphology and the dynamics of photoinduced carriers, which is the scope of this paper.

Flash photolysis time-resolved microwave conductivity (TRMC) is a pump−probe technique to measure the photoconductivity of a film without the need for charge collection at electrical contacts. TRMC is ideal for probing the generation and decay dynamics of photoinduced charge carriers because the microwave photoconductance signal, measured by the photoinduced absorption of the microwave beam, is proportional to the product of the carrier density and the *high-frequency* (typically in the tens of gigahertz) carrier mobility.[38,39] This proportionality provides a straightforward framework in which to understand the influence of morphology on the photoconductance signal. It is reasonable to suggest that, on the nanosecond time scale of the TRMC measurement, exciton dissociation in the mixed phase will be very efficient, due to the proximity of fullerenes to the light-absorbing polymer chromophores,[36,40] leading to higher charge densities and increased photoconductance signal strength. However, the fine mixing may also limit the mobility of the electrons in the fullerene network and the photocarrier lifetimes, which would produce a hole-dominated photoconductance signal and more rapid

decay. In contrast, phase separation of polymer and fullerene may increase photocarrier lifetimes by providing a pathway for oppositely charged carriers to escape each other, as has previously been proposed in binary systems of P3HT with inorganic nanoparticles[41] as well as in purely organic bulk heterojunctions.[36,42,43] In addition, segregated fullerene crystals could lead to electron-dominated photoconductance signals because of the high electron mobility in this phase.[44]

Recently, Savenije *et al.* used TRMC to investigate three semicrystalline poly(thienothiophene) derivatives that exhibited either phase segregation or an intimately mixed, intercalated structure when blended with $PC_{61}BM$.[45] They observed efficient photoinduced charge generation in the intercalated systems, with a concomitant faster photocarrier decay—both observations were attributed to the fine mixing in the intercalated case.[45] They proposed that addition of $PC_{61}BM$ in excess of the intercalated amount may be beneficial as it will result in a system with efficient initial charge separation in the intercalated phase, with the excess, non-intercalated fullerene providing a pathway for electrons to be extracted from the active layer in an OPV device. It should be noted that the study of Savenije *et al.* included a single polymer:fullerene weight ratio of 1:1 for all polymers, and it is therefore unlikely that pure fullerene domains coexisted with a mixed, intercalated phase in their samples.

Here we use TRMC to probe photoinduced carrier yield, lifetime, and high-frequency mobility as a function of morphology in the well-characterized, tightly controlled model pBTTT-C_{14}:fullerene donor−acceptor system. Using a single donor polymer and varying the fullerene derivative and weight ratio allows us to compare the photocarrier dynamics in different phases, mixed and separated, of a single material system. Specifically we address the following questions:

(a) Are electrons effectively extracted from the intercalated phase into the fullerene percolation network prior to carrier decay?
(b) Is the photocarrier lifetime limited by the intimate mixing present in the intercalated phase?
(c) Does the presence of pure polymer and pure fullerene domains enhance the lifetime of photocarriers?

In the following, we will use the term *bimolecular crystal*[35] to refer to partially or fully intercalated pBTTT-C_{14} domains. When domains consisting of *pure* polymer and/or fullerene are formed, they will be stated explicitly. By comparing the magnitude of the photoconductance as a function of $PC_{71}BM$ loading, we show direct evidence that the majority of photogenerated electrons reside in the pure $PC_{71}BM$ domains in samples when both intercalated polymer:fullerene and pure fullerene domains are present. This implies that electrons generated in the intercalated phase are efficiently extracted from that phase to the fullerene domains before they recombine with a hole on the polymer in the bimolecular crystal. We discuss the possible mechanisms that may drive this process and its implications on OPV device operation at high fullerene loading when both intercalated and pure fullerene domains are present. We also show that the intercalated phase decreases, but does not severely limit, the decay time of the photoconductance in fully intercalated samples as well as at high fullerene loading ratios when additional pure PCBM domains are formed. Ultimately, the formation of fullerene domains is critical to device operation.[37] Here we propose that the formation of these domains also creates a driving force for electrons to transfer to them from the bimolecular crystal, which is a prerequisite for extraction of electrons through the percolated fullerene network in efficient photovoltaic devices.

RESULTS AND DISCUSSION

The optical attenuation spectra of the films, corrected for scattering and reflection, are shown in Figure 1a. The attenuation spectra of the 1:1 pBTTT-C_{14}:fullerene blends are similar and are dominated by the optical properties of the polymer, which are determined by the local ordering of the polymer chains. In fact, blending of pBTTT-C_{14} with $PC_{71}BM$ seems to result in slightly better ordering of the polymer chains, reflected by the enhanced vibronic structure visible in the absorption spectrum.[46] Additionally, the absorption spectrum of the pBTTT-C_{14}:bis-$PC_{61}BM$ blend resembles that of the neat polymer, indicating that the chains in the polymer domains adopt a very similar structure. To verify these observations, and that intercalation occurs for $PC_{71}BM$ and not for bis-$PC_{61}BM$, XRD patterns were collected for the pBTTT-C_{14}:fullerene films and are presented in Figure 1b.

Figure 1b shows that the peak near 4.17° ($d \sim 21.2$ Å) in the neat polymer shifts to 2.92° ($d \sim 30.5$ Å) in the 1:1 pBTTT-C_{14}:$PC_{71}BM$ blend, indicating an expansion of the distance between the polymer chains in the pBTTT-C_{14}:$PC_{71}BM$ bimolecular crystal and confirming that fullerene intercalation is occurring between the polymer side chains—an increase in the *d* spacing of 9.3 Å is calculated from the peak shift, consistent with fullerene intercalation between the interdigitated side chains of the polymer.[35] Figure 1b also shows that only a small (~0.2°) shift is observed in the pBTTT-C_{14} case when blended 1:1 by weight with bis-$PC_{61}BM$, which is within the error introduced by the sample holder for the experimental geometry at low angles, indicating that bis-$PC_{61}BM$ does not intercalate between the polymer side chains as was observed for bis-$PC_{71}BM$ in previous work.[37]

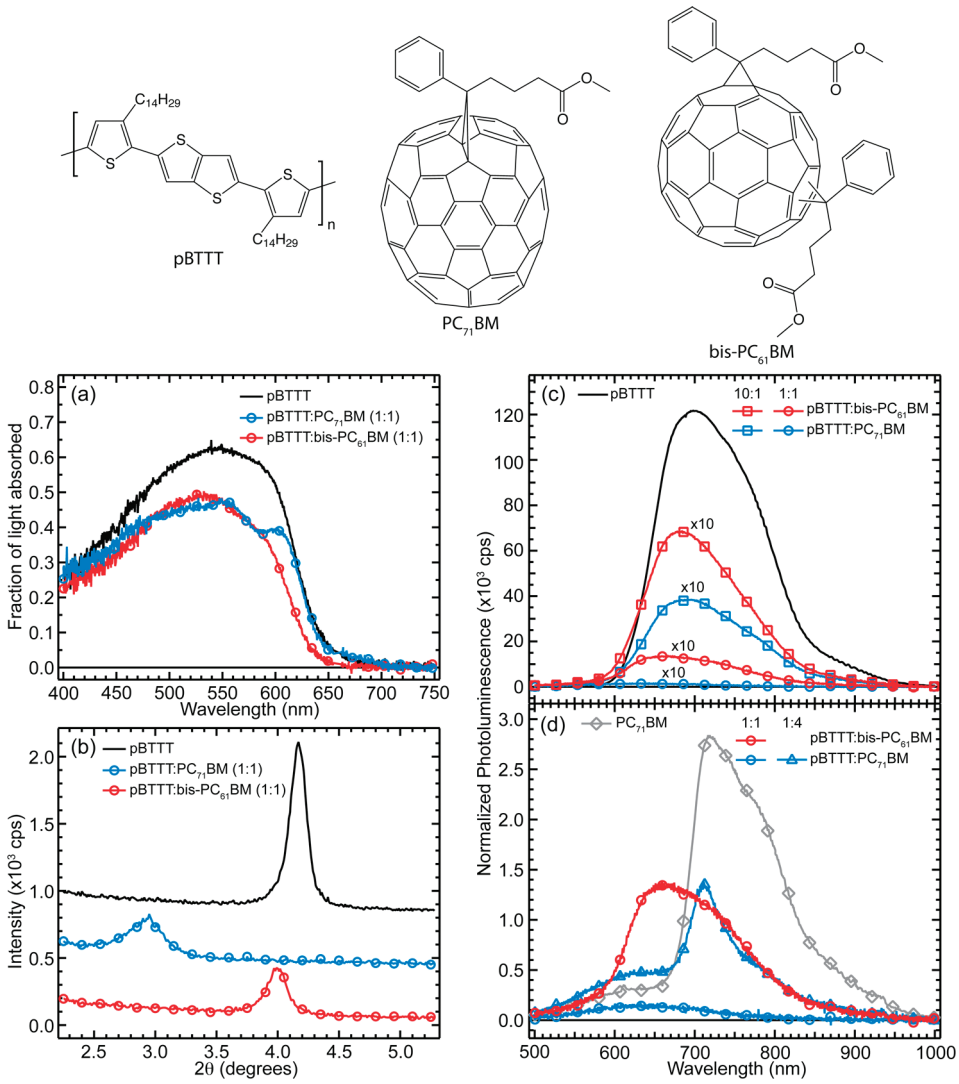

Figure 1. Molecular structures of the pBTTT-C_{14} repeat unit, $PC_{71}BM$, and bis-$PC_{61}BM$. (a) Optical attenuation spectra and (b) XRD patterns of neat pBTTT-C_{14} (black traces), an intercalated 1:1 pBTTT-C_{14}:$PC_{71}BM$ blend (blue traces) and a non-intercalated 1:1 pBTTT-C_{14}:bis-$PC_{61}BM$ blend (red traces): photoluminescence spectra, normalized by the fraction of light absorbed at the excitation wavelength (445 nm), of neat pBTTT-C_{14} (black trace), pBTTT-C_{14}:$PC_{71}BM$ blends (blue traces), pBTTT-C_{14}:bis-$PC_{61}BM$ blends (red traces), and neat $PC_{71}BM$ (gray trace + diamonds) at (a) low and (b) high fullerene loading; 10:1 loading is denoted by squares, 1:1 by circles, and 1:4 by triangles.

The photoluminescence (PL) spectra of films are shown in Figure 1c,d: strong photoluminescence quenching (exceeding 94%) was observed for both pBTTT-C_{14}:$PC_{71}BM$ and pBTTT-C_{14}:bis-$PC_{61}BM$ 10:1 blends (Figure 1c), with the largest quenching (~99%) in the intercalated pBTTT-C_{14}:$PC_{71}BM$ 1:1 blend—it should be noted that the small PL signal observed in the fully intercalated pBTTT-C_{14}:$PC_{71}BM$ blend appears to originate from the quartz substrate used to support the film. This suggests very efficient exciton dissociation due to the donor–acceptor interface even in the phase-separated pBTTT-C_{14}:bis-$PC_{61}BM$ blend. PL decays are shown in Figure 2; as expected, the presence of a fullerene acceptor results in a reduction in the PL lifetime, independent of composition. A comparison of the extent of PL quenching, as measured by steady-state and time-resolved methods, in the context of the contribution from *static* and *dynamic* quenching processes is discussed in conjunction with the TRMC data in detail below.

Interestingly, while very efficient (>99%) quenching was seen in the bimolecular crystal (pBTTT-C_{14}:$PC_{71}BM$ 1:1), PL was observed in the 1:4 blend, as shown in Figure 1d. In the 1:4 blend with $PC_{71}BM$, the polymer is fully intercalated with fullerene, resulting in the formation of pure $PC_{71}BM$ domains outside this mixed phase.[35] Figure 1d shows the similarity between the spectra of the 1:4 pBTTT-C_{14}:$PC_{71}BM$ blend and a drop-cast, neat $PC_{71}BM$ film, indicating that the residual PL spectrum of the 1:4 blend is due to the pure $PC_{71}BM$ domains that are formed outside the bimolecular crystal phase.

Photocarrier dynamics were studied using TRMC, a contactless, pump–probe technique where both the

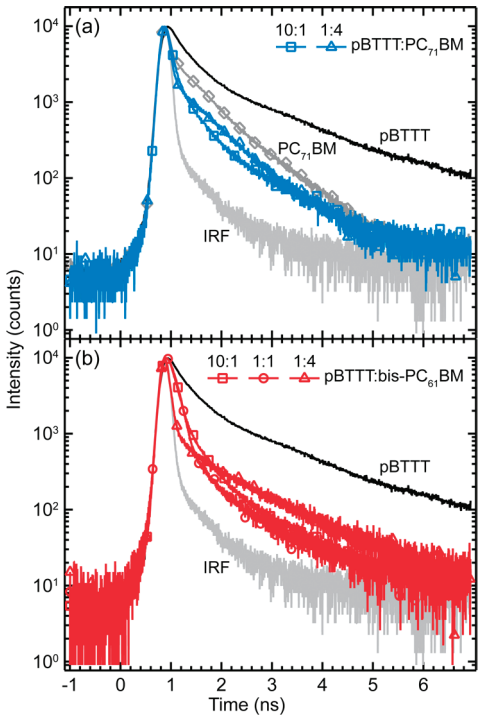

Figure 2. Photoluminescence decays for (a) pBTTT-C_{14}:$PC_{71}BM$ blends (blue traces) and (b) pBTTT-C_{14}:bis-$PC_{61}BM$ blends (red traces)—also shown are the corresponding decays for a neat pBTTT-C_{14} film (black traces) and a neat $PC_{71}BM$ film (gray trace + diamonds), along with the instrument response function (IRF); 10:1 loading is denoted by squares, 1:1 by circles, and 1:4 by triangles.

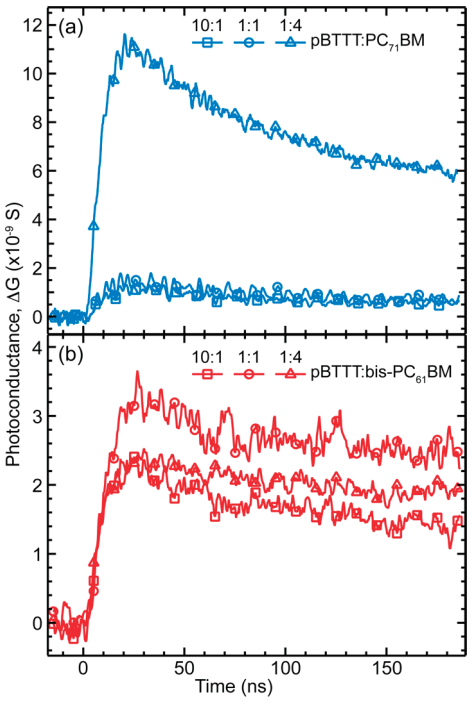

Figure 3. Photoconductance transients of (a) pBTTT-C_{14}:$PC_{71}BM$ blends (blue traces) and (b) pBTTT-C_{14}:bis-$PC_{61}BM$ blends (red traces) after excitation with 5 ns laser pulses at 550 nm; 10:1 loading is denoted by squares, 1:1 by circles, and 1:4 by triangles. The absorbed photon flux was $\sim 10^{12}$ photons/cm^2/pulse.

initial generation of mobile carriers and their eventual decay back to equilibrium are monitored through the time-resolved changes in absorbed microwave power by the sample, which are related to the transient photoconductance, $\Delta G(t)$, by eq 2.[38,47−49] In Figure 3, the transient photoconductance is shown for (a) pBTTT-C_{14}:$PC_{71}BM$ and (b) pBTTT-C_{14}:bis-$PC_{61}BM$ blends at an absorbed photon flux of $\sim 10^{12}$ photons/cm^2/pulse. Comparison between different blends shows a similar magnitude of the peak photoconductance of 10:1 and 1:1 blend with $PC_{71}BM$, while a significant increase is seen for the 1:4 pBTTT-C_{14}:$PC_{71}BM$ sample—a similar increase in the photoconductance was observed in TRMC studies of poly(2,5-bis(3-dodecylthiophen-2-yl)thieno[2,3-*b*]thiophene) (pBTCT-C_{12}) blended with $PC_{61}BM$ upon increasing the weight ratio from 1:1 to 1:4.[50] As we will discuss in detail below, this increase shown in Figure 3a comes from the contribution to the signal of mobile electrons residing in the pure $PC_{71}BM$ domains in the 1:4 blend. By contrast, the photoconductance of pBTTT-C_{14}:bis-$PC_{61}BM$ films exhibits a much weaker dependence on the fullerene loading ratio. In this case, pure fullerene domains form at any loading ratio, meaning that no abrupt change in the photoconductance is observed that would signify the onset of the formation of a new phase. In the following, we discuss these observations regarding the magnitude of the photoconductance in more detail. We also present a comparison of the decay times of the photoconductance of different films and how they correlate to the morphology.

The end-of-pulse (peak) photoconductance, ΔG_{EOP}, can be related to the product of the yield for carrier generation, ϕ, and the sum of the high-frequency electron and hole mobilities in the blend, $\Sigma\mu$, by[38]

$$\Delta G_{EOP} = \beta q_e \times I_0 F_A \times \phi\Sigma\mu \quad (1)$$

where $\beta = 2.2$ is the ratio of the interior dimensions of the waveguide, q_e is the electronic charge, I_0 is the incident photon flux of the excitation pulse, and F_A is the fraction of absorbed photons. The principal figure of merit extracted from TRMC measurements is the product of the yield for free carrier generation and the sum of the high-frequency mobilities of free carriers (electrons and holes), $\phi\Sigma\mu$, which can be calculated from eq 1 using the peak of the photoconductance transients and the known *absorbed* photon flux, I_0F_A. The $\phi\Sigma\mu$ product (peak photoconductance normalized by the absorbed photon flux) as a function of I_0F_A for the pure polymer and for blends with $PC_{71}BM$ and bis-$PC_{61}BM$ is shown in Figure 4. As expected, there is an increase in $\phi\Sigma\mu$ compared to neat pBTTT-C_{14} when either fullerene is added to the blend, due to enhanced exciton dissociation at the donor−acceptor interface (increasing ϕ) and, in some cases, a contribution to $\Sigma\mu$ of the electron mobility in the fullerene,[44,51] as we discuss below.

The decline of $\phi\Sigma\mu$ with increasing light intensity, observed in all samples, is due to higher order loss processes that are only present at high photon fluxes, which in effect reduce ϕ.[49,52] At low intensities, these processes are negligible and $\phi\Sigma\mu$ is expected to reach a plateau, indicating a linear response of the photoinduced carrier density to the incident photon flux. This region is most relevant to OPV devices, as under AM 1.5 illumination an OPV device experiences photon fluxes of *ca.* 10^9 photons/cm^2. The data of Figure 4 do not reach a plateau at low light intensities, except marginally for the pBTTT-C_{14}:PC_{71}BM 1:4 sample. However, there are clear similarities and distinctions between the samples, represented in Figure 5, where $\phi\Sigma\mu$ is shown as a function of PCBM loading at the lowest *common* absorbed photon flux of 10^{12} photons/cm^2/pulse for the blends—cartoons of the morphology as a function of fullerene loading for both pBTTT-C_{14}:PC_{71}BM and pBTTT-C_{14}:bis-PC_{61}BM samples are also shown in Figure 5.

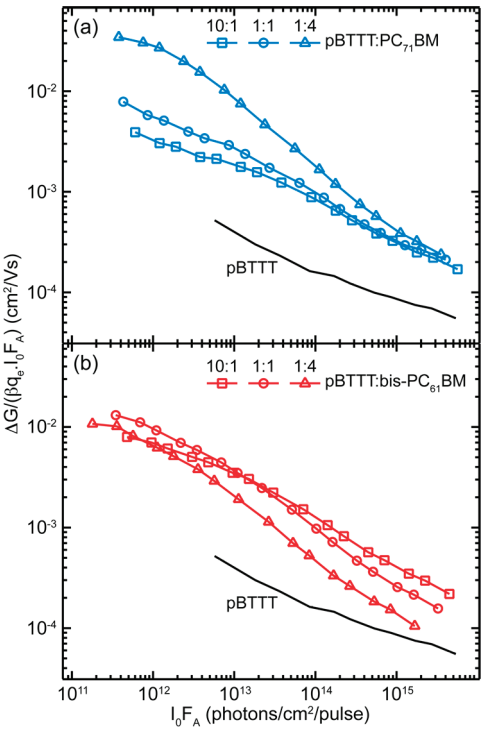

Figure 4. Peak photoconductance, normalized by the absorbed photon flux, *i.e.*, the yield mobility ($\phi\Sigma\mu$) product, for (a) pBTTT-C_{14}:PC_{71}BM blends (blue traces) and (b) pBTTT-C_{14}:bis-PC_{61}BM blends (red traces)—also shown is $\phi\Sigma\mu$ for a neat pBTTT-C_{14} film (black traces); 10:1 loading is denoted by squares, 1:1 by circles, and 1:4 by triangles.

Figure 5a shows a rise in $\phi\Sigma\mu$ from the neat polymer to the 10:1 pBTTT-C_{14}:PC_{71}BM blend, due to enhanced exciton dissociation in the fullerene-containing bimolecular crystal. In this case, the polymer is not fully intercalated[35] and it is reasonable to assume that fullerenes are dispersed enough in the bimolecular crystal that they do not form a continuous network to facilitate electron percolation. However, exciton dissociation is still efficient in this case, as evidenced by the ~95% quenching of the PL (Figure 1c). Time-resolved PL (TRPL) measurements (Figure 2a) on the same samples as used for TRMC yield an average exciton lifetime of $\tau_n \approx 950$ ps in neat pBTTT-C_{14} film and $\tau_b \approx 290$ ps in the 10:1 pBTTT-C_{14}:PC_{71}BM blend. The decrease in the exciton lifetime in the blend is caused by turning on

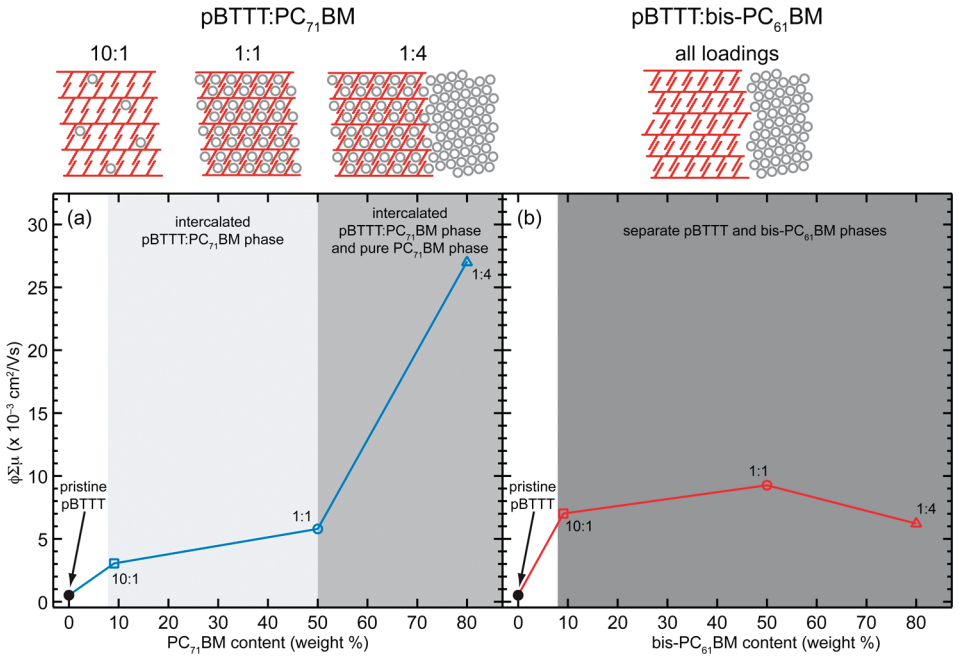

Figure 5. Yield mobility ($\phi\Sigma\mu$) product plotted *versus* fullerene content for blends containing either (a) the intercalated PC_{71}BM phase or (b) the non-intercalated bis-PC_{61}BM phase—the points were taken at an absorbed photon flux of ~10^{12} photons/cm^2/pulse: cartoons of the different morphologies are also shown above the data for reference.

additional exciton deactivation pathways, such as exciton quenching as a result of electron transfer to $PC_{71}BM$, that compete with intrinsic exciton decay processes in the neat polymer. From the exciton lifetimes, a lower limit of the yield for free carrier generation, ϕ, in the 10:1 pBTTT-C_{14}:$PC_{71}BM$ film can be estimated as $\phi \geq 1 - (\tau_b/\tau_n) = 0.70$. We consider this a lower limit on the basis that (a) the steady-state PL data suggest a larger degree of exciton quenching than is implied by the reduction in the exciton lifetime, indicating that static quenching also plays an important role in the observed PL quenching, and (b) the yield of intrinsic carrier generation in the neat polymer—confirmed by the measurable TRMC signal in Figure 4—has not been accounted for and results in an enhanced carrier yield for the polymer:fullerene blend. Although it is possible that an exciton deactivation pathway may have been opened up that does not lead to free carrier generation, external quantum efficiency (EQE) measurements on devices with a pBTTT-C_{14}:$PC_{71}BM$ active layer suggest that the carrier yield in this system is actually limited by light absorption rather than exciton dissociation.[46] At this low loading ratio, the fullerenes are likely dispersed between the polymer chains; therefore, the sum of the mobilities, $\Sigma\mu$, is expected to be dominated by the hole mobility in the polymer, with negligible contribution from electron mobility in the fullerenes. Baumann *et al.* reached a similar conclusion as a result of the observation of different temperature dependencies for the electron and hole mobilities in pBTCT-C_{12}:$PC_{61}BM$ blends at different fullerene loadings.[50] This consideration allows us to quantify the *high-frequency* hole mobility in pBTTT-C_{14}, as discussed below.

A small increase in $\phi\Sigma\mu$ is observed when the weight ratio is increased to 1:1 pBTTT-C_{14}:$PC_{71}BM$ that can be attributed to two factors. First, the efficiency for exciton dissociation increases, as evidenced by nearly complete (>99%) quenching of the PL. This is expected, as in this case, every polymer repeat unit has fullerenes intercalated on either side of it between the tetradecyl side chains.[35] The absence of measurable PL signal in the 1:1 sample prevents us from measuring the exciton lifetime in this sample. However, on the basis of the above argument, we can estimate ϕ in the 1:1 pBTTT-C_{14}:$PC_{71}BM$ to be in the range $0.70 \leq \phi \leq 1$, where the lower bound is the value estimated for the pBTTT-C_{14}:$PC_{71}BM$ sample with lower fullerene loading. The second factor that could account for the increase in the signal from the 10:1 to the 1:1 pBTTT-C_{14}:$PC_{71}BM$ sample is a non-negligible contribution of the electron mobility to $\Sigma\mu$. Measurements in thin film transistors show that, while no (bulk) electron mobility is measured for blending ratios below 1:1 pBTTT-C_{14}:$PC_{71}BM$, a low but detectable electron mobility is measured at the fully intercalated 1:1 sample.[35] The lowest intensity value for $\phi\Sigma\mu$ in Figure 4 is *ca.* 0.008 $cm^2/(V\cdot s)$, and using the limits for the yield estimated above, $0.008 \leq \Sigma\mu \leq 0.011$ $cm^2/(V\cdot s)$. This range is remarkably close to the value of 0.014 $cm^2/(V\cdot s)$ reported for holes in poly(3-hexylthiophene) (P3HT).[53] Given the similarity of the backbone of the two polymers and considering that both form lamellar structures in films,[54−56] it is reasonable that the high-frequency hole mobility in pBTTT-C_{14} is similar to that in P3HT; therefore, $\Sigma\mu$ as estimated above in the fully intercalated bimolecular crystal should be dominated by the hole mobility in the pBTTT-C_{14}.

The $\phi\Sigma\mu$ product shows a 4-fold increase when the $PC_{71}BM$ loading ratio is increased to 1:4 pBTTT-C_{14}:$PC_{71}BM$. The difference in the structure of the pBTTT-C_{14}:$PC_{71}BM$ 1:4 sample and the pBTTT-C_{14}:$PC_{71}BM$ 1:1 sample is the presence in the former of pure fullerene domains outside of the bimolecular crystal.[35] However, the locus of exciton dissociation and free carrier generation in both the 1:1 and 1:4 blends with $PC_{71}BM$ is the bimolecular crystal because (a) that is where the polymer chromophores are located and (b) the proximity of intercalated fullerene acceptors to the polymer chromophores in the bimolecular crystal favors exciton dissociation there, as opposed to excitons migrating to the interface with the pure fullerene domains. These considerations, in combination with the observed exciton lifetime ($\tau_b \approx 310$ ps) as measured by TRPL (Figure 2a), suggest that ϕ remains high (>0.70) in the pBTTT-C_{14}:$PC_{71}BM$ 1:4 sample and that the increase in $\phi\Sigma\mu$ cannot be attributed solely to a further increase in the yield since that is already within 30% of its upper bound of unity. Therefore, the 4-fold increase of $\phi\Sigma\mu$ shown in Figures 4 and 5 for the pBTTT-C_{14}:$PC_{71}BM$ 1:4 sample can only be attributed to an increase in $\Sigma\mu$. Considering a similar range for the yield as estimated for the pBTTT-C_{14}:$PC_{71}BM$ 1:1 sample, the range for the mobilities in the pBTTT-C_{14}:$PC_{71}BM$ 1:4 film is $0.034 \leq \Sigma\mu \leq 0.047$ $cm^2/(V\cdot s)$, which is at least a factor 3 higher than the value of *ca.* 0.011 $cm^2/(V\cdot s)$ estimated above for the 1:1 blend. Since the morphology of the hole-carrying polymer chains has not changed, the high-frequency hole mobility is expected to be the same in the 1:4 sample and $\Sigma\mu$ must now contain a considerable contribution from the mobility of electrons. The only additional morphological features that can explain this increase in high-frequency electron mobility in the 1:4 sample are the pure $PC_{71}BM$ domains. We also note that energetic considerations previously identified to have a major influence on the efficiency of free carrier generation[27] are not at play in this case because the energy levels of the intercalated phase, where exciton dissociation into free carriers takes place, are the same in the 1:1 and 1:4 samples. Measurements of the high-frequency electron mobility in $PC_{61}BM$ powders using pulse radiolysis TRMC have given values of 0.04−0.3 $cm^2/(V\cdot s)$.[57] Furthermore, values for the local electron mobility in P3HT:$PC_{61}BM$

bulk heterojunctions, estimated from TRMC under optical excitation, range between 0.02 and 0.08 $cm^2/(V \cdot s)$ and correspond to the mobility in pure $PC_{61}BM$ clusters.[44,51,58] These values are comparable to the range of values for $\Sigma\mu$ estimated above for the 1:4 pBTTT-C_{14}:$PC_{71}BM$ sample.

In a previous study, the ultrafast photocarrier dynamics of 1:1 and 1:3 intercalated blends of pBTTT-C_{14} with $PC_{61}BM$ have been investigated.[59] Ultrafast (<120 fs) electron transfer from the polymer to the fullerene upon photoexcitation was observed, with an initial carrier decay process characterized by a time constant of ~200 ps and a signal due to long-lived mobile carriers that persists beyond 1.5 ns.[59] The increase of the transient absorption signal in the 1:3 pBTTT-C_{14}:$PC_{61}BM$ blend, compared to that in the 1:1 sample, was attributed to an increase in photocarrier generation yield, although it should be noted that absolute values of the absorption coefficient of the pBTTT-C_{14} polaron are unknown and little information is known about the effect of morphology (*i.e.*, blending with fullerene) on the absorption coefficient. The combination of a detailed knowledge of the structure, along with the spectroscopy and TRMC techniques used in this study, leads us here to a different conclusion, namely, that the yield is approximately the same in the fully intercalated blend and the blend composed of both fully intercalated polymer:fullerene and pure $PC_{71}BM$ domains, and that the observed difference in the TRMC signal in the sample with $PC_{71}BM$ loading that exceeds full intercalation (1:4 blend) is caused by the contribution of the electron mobility to the photoconductance.

The conclusion that in the 1:4 pBTTT-C_{14}:$PC_{71}BM$ sample $\Sigma\mu$ is dominated by the mobility of electrons in the pure $PC_{71}BM$ domains has significant implications: while electrons are predominately generated by exciton dissociation in the bimolecular crystal, within a few nanoseconds (the duration of the excitation pulse in the TRMC experiment), they transition from the bimolecular crystal to the fullerene domains where the microwave probe detects their high contribution to the sum of the mobilities. This is an ideal scenario for free carrier generation in an exitonic solar cell: a bimolecular crystal efficiently dissociates excitons to free electrons and holes, and the electrons transfer efficiently to pure fullerene domains that form the percolation pathway for electrons to traverse the film and generate photocurrent. Recent work on the structure of pBTTT-C_{14}:$PC_{71}BM$ composites shows that the fullerene cages in the fully intercalated bimolecular crystal are electronically coupled and, therefore, form a channel for electrons to transfer to pure fullerene domains that lie outside the intercalated phase.[60]

The efficient transfer of electrons from the bimolecular crystal to the pure $PC_{71}BM$ domains is suggestive of a driving force for this process. We propose two mechanisms that can promote this electron transfer process, one energetic and one entropic. An extended fullerene domain may promote delocalization of the electron that lowers the carrier energy, which drives carrier transfer from the bimolecular crystal to the pure fullerene domain. Entropic arguments have previously been proposed for exciton dissociation into free carriers at a donor−acceptor interface.[4] Here we modify that argument and propose that during, and shortly after, the laser pulse there is a charge density gradient that drives electrons out of the bimolecular crystal into the pure fullerene domains. As we will discuss below, the latter mechanism is also consistent with the measured photoconductance decay.

As shown in Figure 5b, the $\phi\Sigma\mu$ in the pBTTT-C_{14}:bis-$PC_{61}BM$ does not show abrupt changes with fullerene loading ratio. In this case, no intercalated phase is formed and phase separation gives rise to pure polymer and pure fullerene domains for any weight ratio. The similarity of the morphology for all weight ratios is reflected in the similarity of the values of $\phi\Sigma\mu$: at low excitation intensity, this falls between 0.008 and 0.013 $cm^2/(V \cdot s)$ for all blends. TRPL measurements (Figure 2b) give values of $\tau_b \approx 215$ and 155 ps for the pBTTT-C_{14}:bis-$PC_{61}BM$ 10:1 and 1:1, respectively. The estimated yields are $\phi \geq 0.77$ in the 10:1 and $\phi \geq 0.84$ in the pBTTT-C_{14}:bis-$PC_{61}BM$ 1:1 films, which indicates efficient migration of excitons in pure pBTTT-C_{14} crystallites to the interface between the polymer and bis-$PC_{61}BM$, even in the 10:1 sample. The better agreement between the values for the PL quenching measured using steady-state and time-resolved techniques for the pBTTT-C_{14}:bis-$PC_{61}BM$ blends indicates that *static* quenching plays a less important role in the overall exciton quenching process, which suggests that there are no domains containing intimately mixed, amorphous polymer and fullerene. This observation indicates that the quenching mechanism is dominated by exciton migration to the interface between the pure polymer and fullerene domains, which manifests itself as a *dynamic* quenching process thereby reducing the exciton lifetime.

The results of Figure 5b indicate that $\Sigma\mu$ is almost independent of composition in the blends with bis-$PC_{61}BM$, consistent with fullerene domain formation at all bis-$PC_{61}BM$ loadings.[37] A similar dependence of $\phi\Sigma\mu$ on fullerene loading has recently been observed in phase-separated P3HT:$PC_{61}BM$ blends.[58] The range of values is $0.011 \leq \Sigma\mu \leq 0.015$ $cm^2/(V \cdot s)$, which are slightly larger than the hole mobilities in the pBTTT-C_{14} domains as estimated above for the pBTTT-C_{14}:$PC_{71}BM$ 1:1 sample. It has been shown recently that the pBTTT-C_{14} chains pack closer in the pure polymer domains than in the bimolecular crystal,[60] which may account for a value in the upper end of the mobility range shown above (0.015 $cm^2/(V \cdot s)$) being higher than $\Sigma\mu \leq$ 0.011 $cm^2/(V \cdot s)$ estimated in the fully intercalated bimolecular crystal. However, it is also possible that

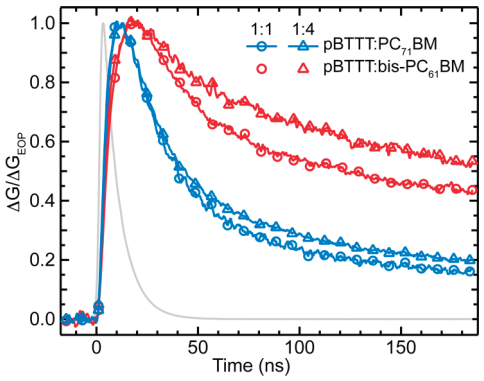

Figure 6. Photoconductance transients, normalized to the peak signal, for blends of pBTTT-C_{14} with $PC_{71}BM$ (blue traces) and bis-$PC_{61}BM$ (red traces); 1:1 loading is denoted by circles and 1:4 by triangles—also shown is a representative instrument response function (gray trace). The absorbed photon flux was $\sim 6 \times 10^{13}$ photons/cm^2/pulse.

the signal in the pBTTT-C_{14}:bis-$PC_{61}BM$ can be attributed both to holes in the polymer and electrons in the bis-$PC_{61}BM$ domains for all compositions—this hypothesis is consistent with the observation by Savenije *et al.* that both free carriers contribute to the photoconductance in phase-separated P3HT:bis-$PC_{61}BM$ blends.[61] These results indicate that the high-frequency electron mobility in bis-$PC_{61}BM$ domains must be smaller than in $PC_{71}BM$ domains, analogous to observations made in preliminary FP-TRMC[61] and photovoltaic device[62] studies of blends of P3HT with the mono- and bisadducts of $PC_{61}BM$.

The effect of blend morphology on the decay times of the photoconductance, as measured by TRMC, is shown in Figure 6, where transients for weight ratios of 1:1 and 1:4 of polymer with $PC_{71}BM$ and bis-$PC_{61}BM$ are compared—the transients are normalized to the peak photoconductance signal. Figure 6 shows that whenever an intercalated phase is present, that is, in the blends with $PC_{71}BM$, the decay of the photoconductance is faster than that observed in the phase-separated blends with bis-$PC_{61}BM$. A faster photoconductance decay for the fully intercalated pBTTT-C_{14}:$PC_{71}BM$ 1:1 blend, compared to the phase-separated pBTTT-C_{14}:bis-$PC_{61}BM$ 1:1 film, is not surprising. In the former, the intimate mixing of the polymer and $PC_{71}BM$ is expected to favor recombination of free carriers. Note, however, that the decay time of the photoconductance of the pBTTT-C_{14}:$PC_{71}BM$ 1:1 blend occurs over several tens of nanoseconds, with significant signal remaining after the 180 ns measurement window, as shown in Figure 6. A short (few nanoseconds) decay time would result in a transient limited by the *ca.* 10 ns response time of the microwave cavity (gray trace in Figure 6) at short times,[39,63] contrary to what is observed here. This implies that free carriers survive well past the duration of the 5 ns laser pulse, and that the free electron has sufficient lifetime to transfer to the pure fullerene domains in the pBTTT-C_{14}:$PC_{71}BM$ 1:4 sample, as discussed above. It is, however, intriguing that the photoconductance lifetime in the pBTTT-C_{14}:$PC_{71}BM$ 1:4 sample is only slightly longer than in the fully intercalated pBTTT-C_{14}:$PC_{71}BM$ 1:1 blend—it should be noted that the transients shown in Figure 6 were chosen for their enhanced signal-to-noise ratio, but that the increase in the photoconductance lifetime was observed at all light intensities.

The modest enhancement of the photconductance lifetime suggests that the locus of recombination is the bimolecular crystal in both samples. Indeed, that is where the holes reside, so an electron in a pure $PC_{71}BM$ domain must, at the very least, transition to the interface with the bimolecular crystal for recombination to occur. After the laser pulse, when charge generation ceases, electrons that remain in the bimolecular crystal recombine with the resident holes; this results in a reversal of the charge density gradient and electrons in the isolated $PC_{71}BM$ domains re-equilibrate (diffuse) to the intercalated phase. The separation of the polymer and fullerene phases in the blends with bis-$PC_{61}BM$ results in longer photoconductance lifetimes, as has been observed in other phase-separated bulk heterojunctions.[39,43,58,64]

Since phase separation in the blends with bis-$PC_{61}BM$ results in a yield for carrier generation per absorbed photon that exceeds 0.77, with a concomitant increase of the photoconductance decay time, the question remains as to whether intercalation of the electron acceptor into the polymer phase is necessary for efficient solar photoconversion. However, the question is not one of *choice* of morphology, as many commonly used polymers, even semicrystalline ones such as P3HT, have an inherently large amorphous fraction[30,33] and it is expected that the fullerene will be effectively dispersed into that fraction,[13,14,23,26,27] even if spatial constraints prohibit intercalation into polymer crystallites.[35] Therefore, an intercalated and/or mixed phase may often be present in bulk heterojunctions with semicrystalline polymers that will play an important role in the dynamics of free carrier generation and recombination.[13,25] Here we use an idealized system, where the intercalated phase is crystalline and its structure is well-characterized, to demonstrate that electrons generated in that phase are efficiently transferred to the isolated fullerene domains, as is required for optimum OPV device performance.[37] Moreover, the photoconductance lifetime is not severely limited by the presence of the intercalated phase. We conclude that electron exchange between intercalated and pure phases in the case of an ordered, intercalated, bimolecular crystal occurs in a direction favorable to device operation as electrons are efficiently transferred outside of the intercalated phase to the percolation network formed by the excess fullerene. Further work is required to determine whether the same observations will prevail in a material system where the intercalated phase is amorphous.

CONCLUSIONS

In summary, efficient exciton quenching is demonstrated for all pBTTT-C_{14}:fullerene systems, independent of composition or the resulting nanomorphology. In the partially and fully intercalated pBTTT-C_{14}:$PC_{71}BM$ systems, 10:1 and 1:1 by weight, respectively, both static and dynamic quenching processes play a role in exciton quenching. In these systems, the electrons are confined to fullerene molecules dispersed in the crystalline polymer domain, resulting in a hole-dominated photoconductance signal and an increased photoconductance decay rate. The addition of excess $PC_{71}BM$ results in the formation of pure fullerene domains that provide a pathway to effective spatial separation of the carriers, which leads to a slight enhancement of the carrier lifetime and a significant contribution to the photoconductance signal due to free electrons in the fullerene domains. The additional solubilizing side chain on bis-$PC_{61}BM$ prevents intercalation in the polymer, resulting in phase separation of the two components. The formation of separate polymer and fullerene domains means that a dynamic process dominates exciton quenching, presumably as a result of exciton diffusion to the donor–acceptor interface. This phase separation results in spatial separation of the carriers, which again reduces the carrier decay rate, independent of composition. The results indicate that intercalation of fullerene into crystalline polymer domains is not detrimental to the generation of long-lived carriers, suggesting that an energetic, or more likely, entropic driving force exists that results in efficient carrier migration from the intercalated phase into the pure fullerene domains. This suggests that efficient organic photovoltaic devices could be fabricated that incorporate intercalated structures in conjuction with pure fullerene domains to facilitate electron extraction.

METHODS

Materials. The polymer poly(2,5-bis(3-tetradecylthiophen-2-yl)thieno[3,2-*b*]thiophene), pBTTT-C_{14}, was synthesized at Imperial College as reported elsewhere.[65] The pBTTT-C_{14} had a number average molecular mass (M_n) of 22 KDa with a polydispersity of 2.0, as determined by gel permeation chromatography in chlorobenzene at 80 °C against polystyrene standards. The fullerene derivatives $PC_{71}BM$ and bis-$PC_{61}BM$ were purchased from Nano-C and Solenne, respectively, and used as received.

Film Preparation and Basic Characterization. For all experiments, films were spin-coated from *ortho*-dichlorobenzene solutions at 1000 rpm for 60 s and subsequently annealed at 180 °C for 10 min. Film deposition and annealing was performed inside a nitrogen-filled glovebox. For X-ray diffraction (XRD) measurements, films were spun onto quartz (Gem Dugout) cut 6° from (0001) that gives low scattering background in XRD. UV–vis absorption, photoluminescence (PL) spectroscopy, and time-resolved microwave conductivity (TRMC) were performed on films spun on plain quartz that was precut to the dimensions of the X-band waveguide used (see below) for TRMC measurements. Film thicknesses were measured using a Veeco Dektak 8 profilometer and ranged from *ca.* 50 to 100 nm. X-ray diffraction measurements were carried out on a Scintag PTS 4-circle goniometer in Bragg–Brentano geometry with Cu Kα radiation.

Steady-State Optical Characterization. The optical attenuation spectra of the films, corrected for scattering and reflection, were measured using a UV–vis spectrophotometer (Ocean Optics HR4000) equipped with an integrating sphere (Ocean Optics ISP-R). The photoluminescence spectra of the films were recorded, after excitation at 445 nm, using a photoluminescence spectrometer (Horiba Jobin-Yvon Fluorolog III) that detected the emission using a liquid nitrogen-cooled CCD.

Time-Resolved Photoluminescence. Photoluminescence decays were recorded, after excitation at 440 nm with a 1 MHz train of pulses (~150 ps fwhm), for emission at 725 nm, with a cooled photon counting photomultiplier tube (Hamamatsu H6279), using the time-correlated single-photon counting technique.[66]

Time-Resolved Microwave Photoconductivity. Photocarrier dynamics were studied using time-resolved microwave photoconductivity (TRMC), a contactless, pump–probe technique where both the initial generation of mobile carriers and their eventual decay back to equilibrium are monitored through the time-resolved changes in absorbed microwave power by the sample.[38,47–49] TRMC measurements were performed at NREL using a system that has been described fully elsewhere.[48,49] Briefly, the sample was placed in an X-band microwave cavity terminated with a grating reflective to microwaves but transparent to the optical excitation that was used to generate carriers within the film. All pBTTT-C_{14}:fullerene films were excited with 5 ns laser pulses at 550 nm from an optical parametric oscillator (Continuum Panther) pumped by a Q-switched Nd:YAG laser (Continuum Powerlite). The transient change in photoconductance, $\Delta G(t)$, was measured *via* changes in the microwave power, $\Delta P(t)$, due to absorption of microwaves by the generated carriers, and is given by

$$\Delta G(t) = -\frac{1}{K}\frac{\Delta P(t)}{P} \quad (2)$$

where K is a calibration factor experimentally determined from the resonance characteristics of the microwave cavity and the dielectric properties of the sample.[48,49,67] The photoconductance, $\Delta G(t)$, probed by TRMC includes the density of free carriers times their mobility, as discussed in eq 1 of the main text. It should be noted that the mobility in eq 1 is the *local* mobility of free carriers (electrons and holes) probed by their absorption of the 9 GHz microwave beam. This *high-frequency* mobility is not necessarily directly related to the mobility determined in bulk (device-type) measurements, where the carrier has to traverse the entire device and the extracted *bulk* mobilities are typically limited by features such as grain boundaries.

Acknowledgment. We thank Jao van de Lagemaat and Obadiah Reid (National Renewable Energy Laboratory, USA), Natalie Stingelin-Stutzmann (Imperial College London, UK), and Mike McGehee (Stanford University, USA) for helpful discussions. The Energy Efficiency & Renewable Energy Solar Energy Technologies Program is acknowledged for the provision of the thin film fabrication and X-ray diffraction facilities. The remainder of this work was funded by the Solar Photochemistry program of the U.S. Department of Energy, Office of Science, Basic Energy Sciences, Division of Chemical Sciences, Geosciences and Biosciences, under Contract No. DE-AC36-08GO28308 to NREL.

REFERENCES AND NOTES

1. Green, M. A.; Emery, K.; Hishikawa, Y.; Warta, W. Solar Cell Efficiency Tables (Version 36). *Prog. Photovoltaics* **2010**, *18*, 346–352.

2. Brabec, C. J.; Gowrisanker, S.; Halls, J. J. M.; Laird, D.; Jia, S.; Williams, S. P. Polymer−Fullerene Bulk-Heterojunction Solar Cells. *Adv. Mater.* **2010**, *22*, 3839–3856.
3. Zhan, X.; Zhu, D. Conjugated Polymers for High-Efficiency Organic Photovoltaics. *Polym. Chem.* **2010**, *1*, 409–419.
4. Clarke, T. M.; Durrant, J. R. Charge Photogeneration in Organic Solar Cells. *Chem. Rev.* **2010**, *110*, 6736–6767.
5. Vak, D.; Kim, S.-S.; Jo, J.; Oh, S.-H.; Na, S.-I.; Kim, J.; Kim, D.-Y. Fabrication of Organic Bulk Heterojunction Solar Cells by a Spray Deposition Method for Low-Cost Power Generation. *Appl. Phys. Lett.* **2007**, *91*, 081102.
6. Green, R.; Morfa, A.; Ferguson, A. J.; Kopidakis, N.; Rumbles, G.; Shaheen, S. E. Performance of Bulk Heterojunction Photovoltaic Devices Prepared by Airbrush Spray Deposition. *Appl. Phys. Lett.* **2008**, *92*, 033301.
7. Steirer, K. X.; Reese, M. O.; Rupert, B. L.; Kopidakis, N.; Olson, D. C.; Collins, R. T.; Ginley, D. S. Ultrasonic Spray Deposition for Production of Organic Solar Cells. *Sol. Energy Mater. Sol. Cells* **2009**, *93*, 447–453.
8. Shaheen, S. E.; Radspinner, R.; Peyghambarian, N.; Jabbour, G. E. Fabrication of Bulk Heterojunction Plastic Solar Cells by Screen Printing. *Appl. Phys. Lett.* **2001**, *79*, 2996–2998.
9. Schilinsky, P.; Waldauf, C.; Brabec, C. J. Performance Analysis of Printed Bulk Heterojunction Solar Cells. *Adv. Funct. Mater.* **2006**, *16*, 1669–1672.
10. Mayer, A. C.; Scully, S. R.; Hardin, B. E.; Rowell, M. W.; McGehee, M. D. Polymer-Based Solar Cells. *Mater. Today* **2007**, *10*, 28–33.
11. Gregg, B. A. Excitonic Solar Cells. *J. Phys. Chem. B* **2003**, *107*, 4688–4698.
12. Gregg, B. A. The Photoconversion Mechanism of Excitonic Solar Cells. *MRS Bull.* **2005**, *30*, 20–22.
13. Parkinson, P.; Lloyd-Hughes, J.; Johnston, M. B.; Herz, L. M. Efficient Generation of Charges *via* Below-Gap Photoexcitation of Polymer-Fullerene Blend Films Investigated by Terahertz Spectroscopy. *Phys. Rev. B* **2008**, *78*, 115321.
14. Piris, J.; Dykstra, T. E.; Bakulin, A. A.; van Loosdrecht, P. H. M.; Knulst, W.; Trinh, M. T.; Schins, J. M.; Siebbeles, L. D. A. Photogeneration and Ultrafast Dynamics of Excitons and Charges in P3HT/PCBM Blends. *J. Phys. Chem. C* **2009**, *113*, 14500–14506.
15. Pingree, L. S. C.; Reid, O. G.; Ginger, D. S. Electrical Scanning Probe Microscopy on Active Organic Electronic Devices. *Adv. Mater.* **2009**, *21*, 19–28.
16. Pingree, L. S. C.; Reid, O. G.; Ginger, D. S. Imaging the Evolution of Nanoscale Photocurrent Collection and Transport Networks during Annealing of Polythiophene/Fullerene Solar Cells. *Nano Lett.* **2009**, *9*, 2946–2952.
17. Germack, D. S.; Chan, C. K.; Kline, R. J.; Fischer, D. A.; Gundlach, D. J.; Toney, M. F.; Richter, L. J.; DeLongchamp, D. M. Interfacial Segregation in Polymer/Fullerene Blend Films for Photovoltaic Devices. *Macromolecules* **2010**, *43*, 3828–3836.
18. Müller, C.; Ferenczi, T. A. M.; Campoy-Quiles, M.; Frost, J. M.; Bradley, D. D. C.; Smith, P.; Stingelin-Stutzmann, N.; Nelson, J. Binary Organic Photovoltaic Blends: A Simple Rationale for Optimum Compositions. *Adv. Mater.* **2008**, *20*, 3510–3515.
19. Hoppe, H.; Sariciftci, N. S. Morphology of Polymer/Fullerene Bulk Heterojunction Solar Cells. *J. Mater. Chem.* **2006**, *16*, 45–61.
20. Yu, G.; Gao, J.; Hummelen, J. C.; Wudl, F.; Heeger, A. J. Polymer Photovoltaic Cells: Enhanced Efficiencies *via* a Network of Internal Donor−Acceptor Heterojunctions. *Science* **1995**, *270*, 1789–1791.
21. Gao, J.; Hide, F.; Wang, H. Efficient Photodetectors and Photovoltaic Cells from Composites of Fullerenes and Conjugated Polymers: Photoinduced Electron Transfer. *Synth. Met.* **1997**, *84*, 979–980.
22. Shaheen, S. E.; Brabec, C. J.; Sariciftci, N. S.; Padinger, F.; Fromherz, T.; Hummelen, J. C. 2.5% Efficient Organic Plastic Solar Cells. *Appl. Phys. Lett.* **2001**, *78*, 841–843.
23. van Duren, J. K. J.; Yang, X. N.; Loos, J.; Bulle-Lieuwma, C. W. T.; Sieval, A. B.; Hummelen, J. C.; Janssen, R. A. J. Relating the Morphology of Poly(*p*-phenylene vinylene)/Methanofullerene Blends to Solar-Cell Performance. *Adv. Funct. Mater.* **2004**, *14*, 425–434.
24. Hoppe, H.; Niggemann, M.; Winder, C.; Kraut, J.; Hiesgen, R.; Hinsch, A.; Meissner, D.; Sariciftci, N. S. Nanoscale Morphology of Conjugated Polymer/Fullerene-Based Bulk-Heterojunction Solar Cells. *Adv. Funct. Mater.* **2004**, *14*, 1005–1011.
25. Yang, X. N.; Loos, J.; Veenstra, S. C.; Verhees, W. J. H.; Wienk, M. M.; Kroon, J. M.; Michels, M. A. J.; Janssen, R. A. J. Nanoscale Morphology of High-Performance Polymer Solar Cells. *Nano Lett.* **2005**, *5*, 579–583.
26. Kline, R. J.; McGehee, M. D. Morphology and Charge Transport in Conjugated Polymer. *Polym. Rev.* **2006**, *46*, 27–45.
27. Ohkita, H.; Cook, S.; Astuti, Y.; Duffy, W.; Tierney, S.; Zhang, W.; Heeney, M.; McCulloch, I.; Nelson, J.; Bradley, D. D. C.; *et al.* Charge Carrier Formation in Polythiophene/Fullerene Blend Films Studied by Transient Absorption Spectroscopy. *J. Am. Chem. Soc.* **2008**, *130*, 3030–3042.
28. Erb, T.; Zhokhavets, U.; Gobsch, G.; Raleva, S.; Stuhn, B.; Schilinsky, P.; Waldauf, C.; Brabec, C. J. Correlation between Structural and Optical Properties of Composite Polymer/Fullerene Films for Organic Solar Cells. *Adv. Funct. Mater.* **2005**, *15*, 1193–1196.
29. Kim, Y.; Cook, S.; Tuladhar, S. M.; Choulis, S. A.; Nelson, J.; Durrant, J. R.; Bradley, D. D. C.; Giles, M.; McCulloch, I.; Ha, C. S.; *et al.* A Strong Regioregularity Effect in Self-Organizing Conjugated Polymer Films and High-Efficiency Polythiophene:Fullerene Solar Cells. *Nat. Mater.* **2006**, *5*, 197–203.
30. Moulé, A. J.; Meerholz, K. Morphology Control in Solution-Processed Bulk-Heterojunction Solar Cell Mixtures. *Adv. Funct. Mater.* **2009**, *19*, 3028–3036.
31. Nieuwendaal, R. C.; Snyder, C. R.; Kline, R. J.; Lin, E. K.; VanderHart, D. L.; DeLongchamp, D. M. Measuring the Extent of Phase Separation in Poly-3-hexylthiophene/Phenyl-C_{61}-Butyric Acid Methyl Ester Photovoltaic Blends with ^{1}H Spin Diffusion NMR Spectroscopy. *Chem. Mater.* **2010**, *22*, 2930–2936.
32. Kim, J. Y.; Kim, S. H.; Lee, H. H.; Lee, K.; Ma, W. L.; Gong, X.; Heeger, A. J. New Architecture for High-Efficiency Polymer Photovoltaic Cells Using Solution-Based Titanium Oxide as an Optical Spacer. *Adv. Mater.* **2006**, *18*, 572–576.
33. Collins, B. A.; Gann, E.; Guignard, L.; He, X.; McNeill, C. R.; Ade, H. Molecular Miscibility of Polymer−Fullerene Blends. *J. Phys. Chem. Lett.* **2010**, *1*, 3160–3166.
34. Treat, N. D.; Brady, M. A.; Smith, G.; Toney, M. F.; Kramer, E. J.; Hawker, C. J.; Chabinyc, M. L. Interdiffusion of PCBM and P3HT Reveals Miscibility in a Photovoltaically Active Blend. *Adv. Energy Mater.* **2011**, *1*, 82–89.
35. Mayer, A. C.; Toney, M. F.; Scully, S. R.; Rivnay, J.; Brabec, C. J.; Scharber, M.; Koppe, M.; Heeney, M.; McCulloch, I.; McGehee, M. D. Bimolecular Crystals of Fullerenes in Conjugated Polymers and the Implications of Molecular Mixing for Solar Cells. *Adv. Funct. Mater.* **2009**, *19*, 1173–1179.
36. Keivanidis, P. E.; Clarke, T. M.; Lilliu, S.; Agostinelli, T.; Macdonald, J. E.; Durrant, J. R.; Bradley, D. D. C.; Nelson, J. Dependence of Charge Separation Efficiency on Film Microstructure in Poly(3-hexylthiophene-2,5-diyl):[6,6]-Phenyl-C_{61} Butyric Acid Methyl Ester Blend Films. *J. Phys. Chem. Lett.* **2010**, *1*, 734–738.
37. Cates, N. C.; Gysel, R.; Beiley, Z.; Miller, C. E.; Toney, M. F.; Heeney, M.; McCulloch, I.; McGehee, M. D. Tuning the Properties of Polymer Bulk Heterojunction Solar Cells by Adjusting Fullerene Size To Control Intercalation. *Nano Lett.* **2009**, *9*, 4153–4157.
38. Dicker, G.; de Haas, M. P.; Siebbeles, L. D. A.; Warman, J. M. Electrodeless Time-Resolved Microwave Conductivity Study of Charge-Carrier Photogeneration in Regioregular Poly(3-hexylthiophene) Thin Films. *Phys. Rev. B* **2004**, *70*, 045203.
39. Ferguson, A. J.; Blackburn, J. L.; Holt, J. M.; Kopidakis, N.; Tenent, R. C.; Barnes, T. M.; Heben, M. J.; Rumbles, G. Photoinduced Energy and Charge Transfer in P3HT:SWNT Composites. *J. Phys. Chem. Lett.* **2010**, *1*, 2406–2411.

40. Ballantyne, A. M.; Ferenczi, T. A. M.; Campoy-Quiles, M.; Clarke, T. M.; Maurano, A.; Wong, K. H.; Zhang, W.; Stingelin-Stutzmann, N.; Kim, J.-S.; Bradley, D. D. C.; *et al.* Understanding the Influence of Morphology on Poly(3-hexylselenothiophene):PCBM Solar Cells. *Macromolecules* **2010**, *43*, 1169–1174.
41. Dayal, S.; Reese, M. O.; Ferguson, A. J.; Ginley, D. S.; Rumbles, G.; Kopidakis, N. The Effect of Nanoparticle Shape on the Photocarrier Dynamics and Photovoltaic Device Performance of Poly(3-hexylthiophene):CdSe Nanoparticle Bulk Heterojunction Solar Cells. *Adv. Funct. Mater.* **2010**, *20*, 2629–2635.
42. Hamilton, R.; Shuttle, C. G.; O'Regan, B.; Hammant, T. C.; Nelson, J.; Durrant, J. R. Recombination in Annealed and Nonannealed Polythiophene/Fullerene Solar Cells: Transient Photovoltage Studies *versus* Numerical Modeling. *J. Phys. Chem. Lett.* **2010**, *1*, 1432–1436.
43. Rance, W. L.; Rupert, B. L.; Mitchell, W. J.; Köse, M. E.; Ginley, D. S.; Shaheen, S. E.; Rumbles, G.; Kopidakis, N. Conjugated Thiophene Dendrimer with an Electron-Withdrawing Core and Electron-Rich Dendrons: How the Molecular Structure Affects the Morphology and Performance of Dendrimer: Fullerene Photovoltaic Devices. *J. Phys. Chem. C* **2010**, *114*, 22269–22276.
44. Grzegorczyk, W. J.; Savenije, T. J.; Dykstra, T. E.; Piris, J.; Schins, J. M.; Siebbeles, L. D. A. Temperature-Independent Charge Carrier Photogeneration in P3HT−PCBM Blends with Different Morphology. *J. Phys. Chem. C* **2010**, *114*, 5182–5186.
45. Savenije, T. J.; Grzegorczyk, W. J.; Heeney, M.; Tierney, S.; McCulloch, I.; Siebbeles, L. D. A. Photoinduced Charge Carrier Generation in Blends of Poly(thienothiophene) Derivatives and [6,6]-Phenyl-C_{61}-Butyric Acid Methyl Ester: Phase Segregation *versus* Intercalation. *J. Phys. Chem. C* **2010**, *114*, 15116–15120.
46. Parmer, J. E.; Mayer, A. C.; Hardin, B. E.; Scully, S. R.; McGehee, M. D.; Heeney, M.; McCulloch, I. Organic Bulk Heterojunction Solar Cells Using Poly(2,5-bis(3-tetradecylthiophen-2-yl)thieno[3,2,-*b*]thiophene. *Appl. Phys. Lett.* **2008**, *92*, 113309.
47. Kroeze, J. E.; Savenije, T. J.; Vermeulen, M. J. W.; Warman, J. M. Contactless Determination of the Photoconductivity Action Spectrum, Exciton Diffusion Length, and Charge Separation Efficiency in Polythiophene-Sensitized TiO_2 Bilayers. *J. Phys. Chem. B* **2003**, *107*, 7696–7705.
48. Piris, J.; Kopidakis, N.; Olson, D. C.; Shaheen, S. E.; Ginley, D. S.; Rumbles, G. The Locus of Free Charge-Carrier Generation in Solution-Cast $Zn_{1-x}Mg_xO$/Poly(3-hexylthiophene) Bilayers for Photovoltaic Applications. *Adv. Funct. Mater.* **2007**, *17*, 3849–3857.
49. Ferguson, A. J.; Kopidakis, N.; Shaheen, S. E.; Rumbles, G. Quenching of Excitons by Holes in Poly(3-hexylthiophene) Films. *J. Phys. Chem. C* **2008**, *112*, 9865–9871.
50. Baumann, A.; Savenije, T. J.; Murthy, D. H. K.; Heeney, M.; Dyakonov, V.; Deibel, C. Influence of Phase Segregation on Recombination Dynamics in Organic Bulk-Heterojunction Solar Cells. *Adv. Funct. Mater.* 2011, doi: 10.1002/adfm.201002358.
51. Savenije, T. J.; Kroeze, J. E.; Wienk, M. M.; Kroon, J. M.; Warman, J. M. Mobility and Decay Kinetics of Charge Carriers in Photoexcited PCBM/PPV Blends. *Phys. Rev. B* **2004**, *69*, 155205.
52. Dicker, G.; de Haas, M. P.; Siebbeles, L. D. A. Signature of Exciton Annihilation in the Photoconductance of Regioregular Poly(3-hexylthiophene). *Phys. Rev. B* **2005**, *71*, 155204.
53. Dicker, G.; de Haas, M. P.; Warman, J. M.; de Leeuw, D. M.; Siebbeles, L. D. A. The Disperse Charge-Carrier Kinetics in Regioregular Poly(3-hexylthiophene). *J. Phys. Chem. B* **2004**, *108*, 17818–17824.
54. Kline, R. J.; DeLongchamp, D. M.; Fischer, D. A.; Lin, E. K.; Richter, L. J.; Chabinyc, M. L.; Toney, M. F.; Heeney, M.; McCulloch, I. Critical Role of Side-Chain Attachment Density on the Order and Device Performance of Polythiophenes. *Macromolecules* **2007**, *40*, 7960–7965.
55. DeLongchamp, D. M.; Kline, R. J.; Jung, Y.; Lin, E. K.; Fischer, D. A.; Gundlach, D. J.; Cotts, S. K.; Moad, A. J.; Richter, L. J.; Toney, M. F.; *et al.* Molecular Basis of Mesophase Ordering in a Thiophene-Based Copolymer. *Macromolecules* **2008**, *41*, 5709–5715.
56. DeLongchamp, D. M.; Kline, R. J.; Jung, Y.; Germack, D. S.; Lin, E. K.; Moad, A. J.; Richter, L. J.; Toney, M. F.; Heeney, M.; McCulloch, I. Controlling the Orientation of Terraced Nanoscale "Ribbons" of a Poly(thiophene) Semiconductor. *ACS Nano* **2009**, *3*, 780–787.
57. de Haas, M. P.; Warman, J. M.; Anthopoulos, T. D.; de Leeuw, D. M. The Mobility and Decay Kinetics of Charge Carriers in Pulse-Ionized Microcrystalline PCBM Powder. *Adv. Funct. Mater.* **2006**, *16*, 2274–2280.
58. Ferguson, A. J.; Kopidakis, N.; Shaheen, S. E.; Rumbles, G. Dark Carriers, Trapping, and Activation Control of Carrier Recombination in Neat P3HT and P3HT:PCBM Blends. 2011, submitted.
59. Hwang, I.-W.; Kim, J. Y.; Cho, S.; Yuen, J.; Coates, N.; Lee, K.; Heeney, M.; McCulloch, I.; Moses, D.; Heeger, A. J. Bulk Heterojunction Materials Composed of Poly(2,5-bis(3-tetradecylthiophen-2-yl)thieno[3,2-*b*]thiophene): Ultrafast Electron Transfer and Carrier Recombination. *J. Phys. Chem. C* **2008**, *112*, 7853–7857.
60. Gysel, R.; Cho, E.; Cates-Miller, N.; Risko, C.; Kim, D.; Miller, C. E.; Richter, L. J.; Kline, R. J.; Heeney, M.; McCulloch, I. *et al.* Molecular Packing in a Polymer-Fullerene Bimolecular Crystal, 2011, submitted.
61. Savenije, T. J. Personal communication, 2011.
62. Lenes, M.; Shelton, S. W.; Sieval, A. B.; Kronholm, D. F.; Hummelen, J. C.; Blom, P. W. M. Electron Trapping in Higher Adduct Fullerene-Based Solar Cells. *Adv. Funct. Mater.* **2009**, *19*, 3002–3007.
63. Piris, J.; Ferguson, A. J.; Blackburn, J. L.; Norman, A. G.; Rumbles, G.; Selmarten, D. C.; Kopidakis, N. Efficient Photoinduced Charge Injection from Chemical Bath Deposited CdS into Mesoporous TiO_2 Probed with Time-Resolved Microwave Conductivity. *J. Phys. Chem. C* **2008**, *112*, 7742–7749.
64. Savenije, T. J.; Kroeze, J. E.; Yang, X. N.; Loos, J. The Effect of Thermal Treatment on the Morphology and Charge Carrier Dynamics in a Polythiophene−Fullerene Bulk Heterojunction. *Adv. Funct. Mater.* **2005**, *15*, 1260–1266.
65. McCulloch, I.; Heeney, M.; Bailey, C.; Genevicius, K.; MacDonald, I.; Shkunov, M.; Sparrowe, D.; Tierney, S.; Wagner, R.; Zhang, W. M.; *et al.* Liquid-Crystalline Semiconducting Polymers with High Charge-Carrier Mobility. *Nat. Mater.* **2006**, *5*, 328–333.
66. Phillips, D.; O'Connor, D. V. *Time-Correlated Single-Photon Counting*; Academic Press: London, 1984.
67. Savenije, T. J.; de Haas, M. P.; Warman, J. M. The Yield and Mobility of Charge Carriers in Smooth and Nanoporous TiO_2 Films. *Z. Phys. Chem.* **1999**, *212*, 201–206.